Electronic Supplementary Material (ESI) for Nanoscale.

InTeI: a novel wide-bandgap 2D material with desirable stability and highly anisotropic carrier mobility

Shujuan Jiang,[a] Jingyu Li,[a] Weizhen Chen,[a] Huabing Yin,[*a] Guang-Ping Zheng, [†b] and Yuanxu Wang,[a]

[a.] *Institute for Computational Materials Science, School of Physics and Electronics, Henan University, Kaifeng 475004, China.*

[b.] *Department of Mechanical Engineering, The Hong Kong Polytechnic University, Hung Hom, Kowloon, Hong Kong 999077, China.*

E-mails: [*]yhb@henu.edu.cn (H. Yin); [†]mmzheng@polyu.edu.hk (G.-P. Zheng)

Table S1 Optimized lattice parameters, bond lengths, and calculated HSE06 energy bandgaps (E_g) of bulk and 2D InTeI. The lattice parameters in parentheses are experimental values of bulk InTeI. The quasi-direct bandgaps are obtained at the Γ point.

	Lattice parameters				Bond length		Bandgap E_g (eV)	
N_L	a (Å)	b (Å)	c (Å)	β	$d_{\text{In-Te}}$ (Å)	$d_{\text{In-I}}$ (Å)	Indirect	Quasi-direct
1L	8.56	7.85			2.85~2.90	2.76	2.735	2.763
2L	8.45	7.80			2.82~2.88	2.76	2.581	2.588
3L	8.47	7.79			2.83~2.88	2.76	2.501	2.515
4L	8.48	7.79			2.83~2.88	2.76	2.445	2.469
5L	8.49	7.79			2.83~2.88	2.76	2.400	2.433
Bulk	8.52	7.77	8.05	117.33˚	2.82~2.88	2.76		2.320
Bulk (exp.)	8.41	7.73	8.08	117.03˚				

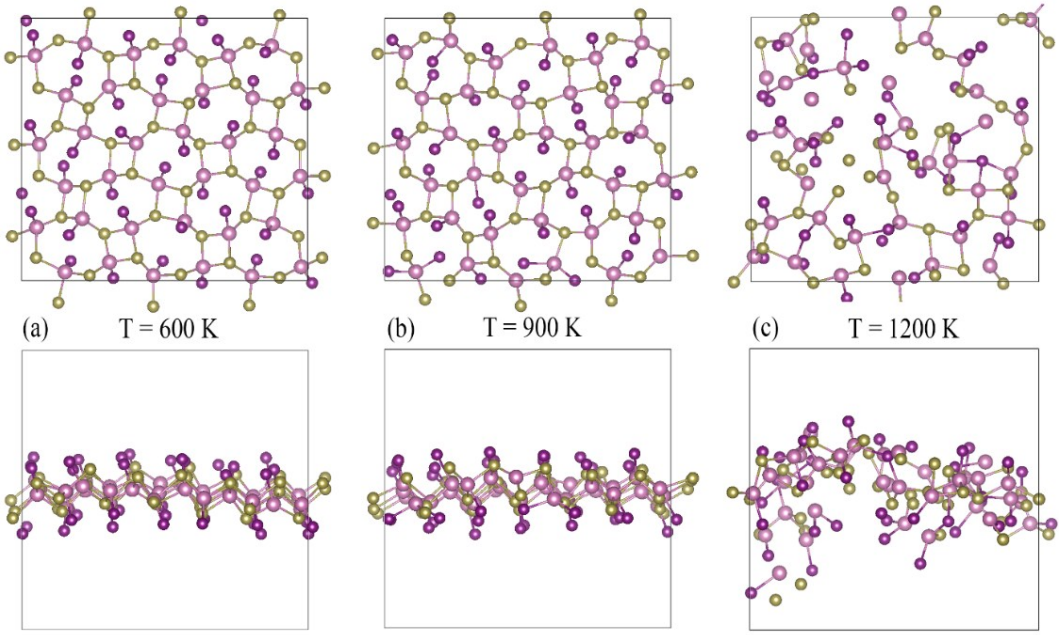

Fig. S1 Top and side views of monolayer InTeI simulated with AIMD at 600 K (a), 900K (b), and 1200K (c), respectively.

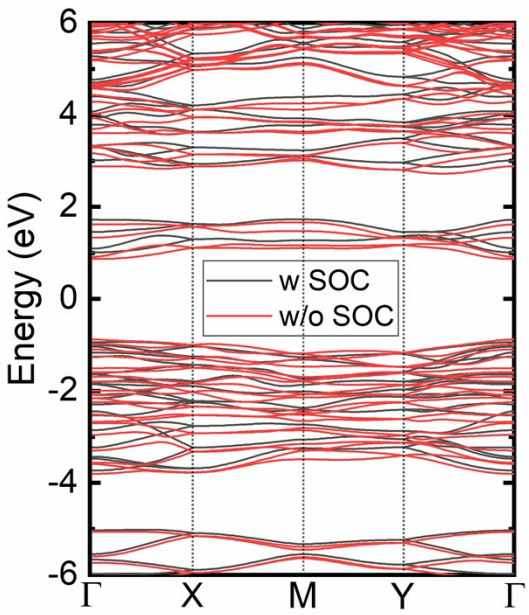

Fig. S2 Band structures of InTeI monolayers based on PBE with (black line) and without (red line) the spin-orbit coupling (SOC) effect. The Fermi levels are set as 0 eV.

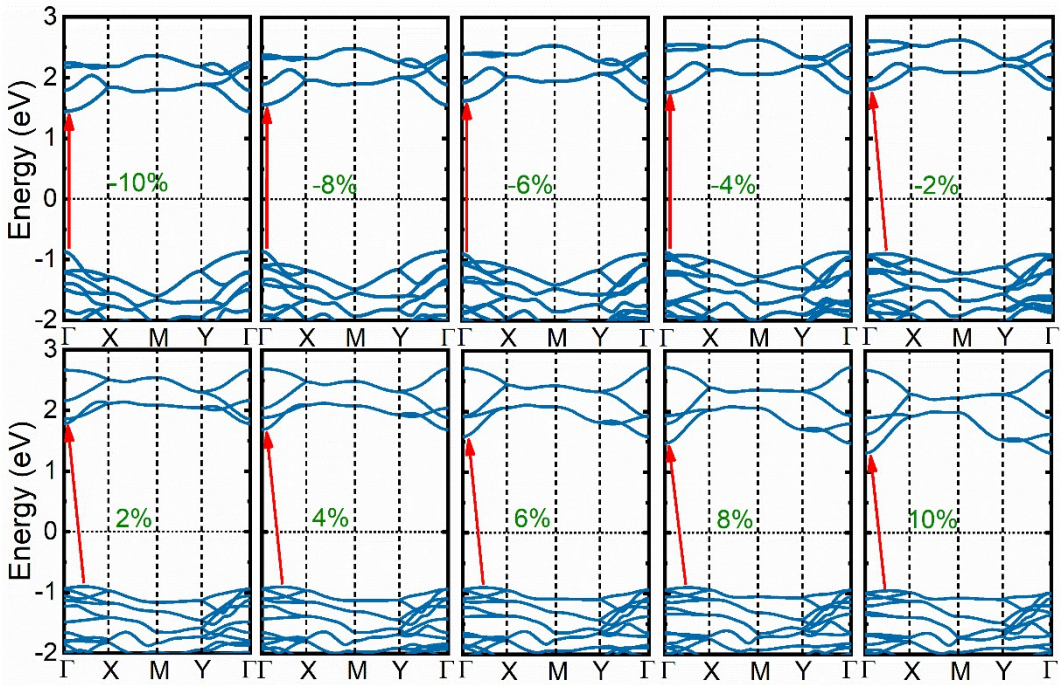

Fig. S3 HSE06 band structures of InTeI monolayer under the in-plane uniaxial strains varying from −10% to 10% along *x*-direction. The strain is defined as $\varepsilon = (a - a_0)/a_0$, where a_0 is the in-plane lattice constant along *x*-direction and a is that under an external strain. The band gaps are highlighted in red. The Fermi level is at 0 eV.

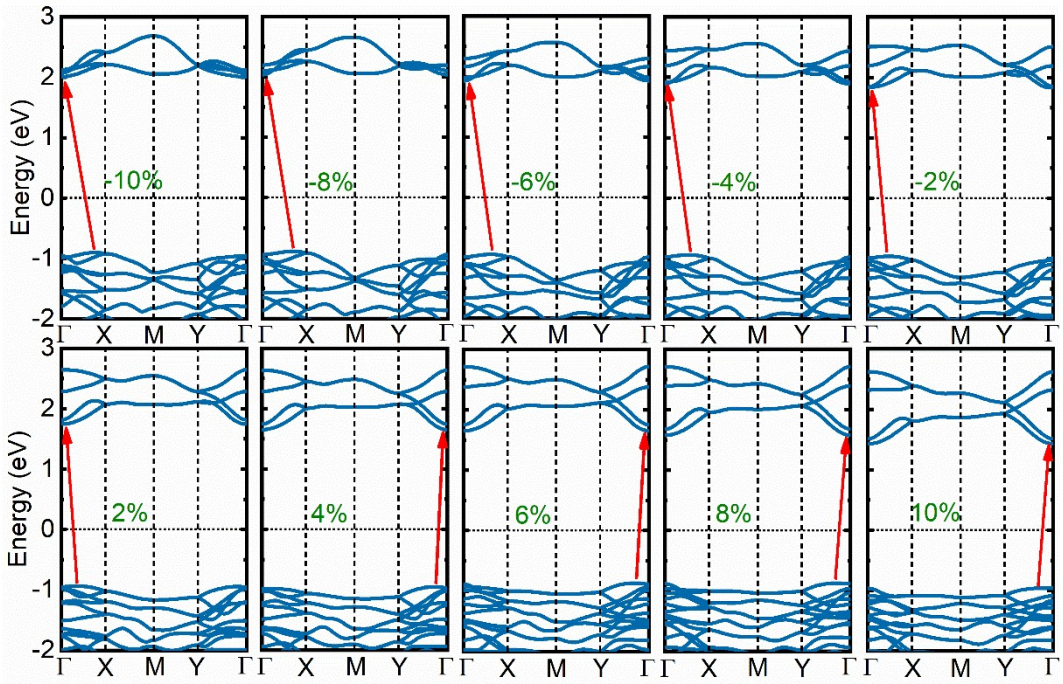

Fig. S4 HSE06 band structures of InTeI monolayer under the in-plane uniaxial strains varying from −10% to 10% along *y*-direction. The strain is defined as $\varepsilon = (b - b_0)/b_0$, where b_0 is the in-plane lattice constant along *y*-direction and *b* is that under an external strain. The band gaps are highlighted in red. The Fermi level is at 0 eV.

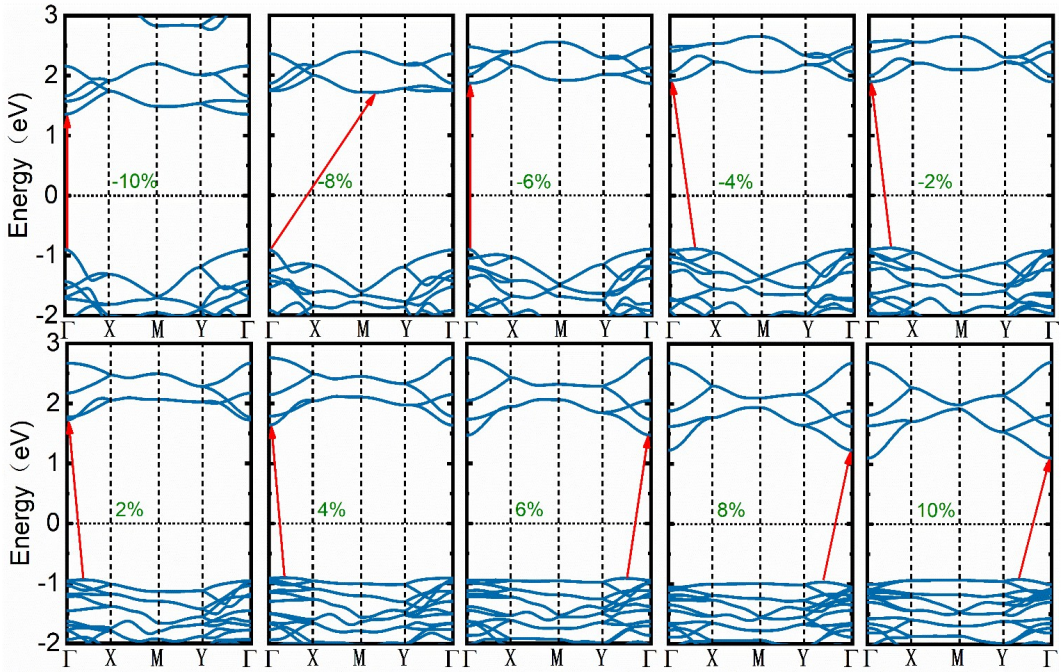

Fig. S5 HSE06 band structures of InTeI monolayer under the biaxial strains varying from −10% to 10% at the *xy*-plane. The band gaps are highlighted in red. The Fermi level is at 0 eV.

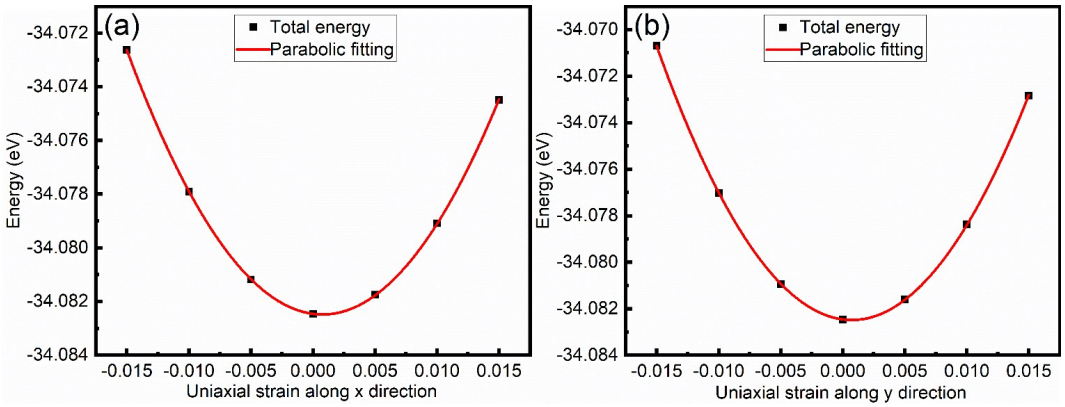

Fig. S6 The total energy of monolayer InTeI as a function of the uniaxial strain applied along (a) *x*-direction, and (b) *y*-direction, respectively.

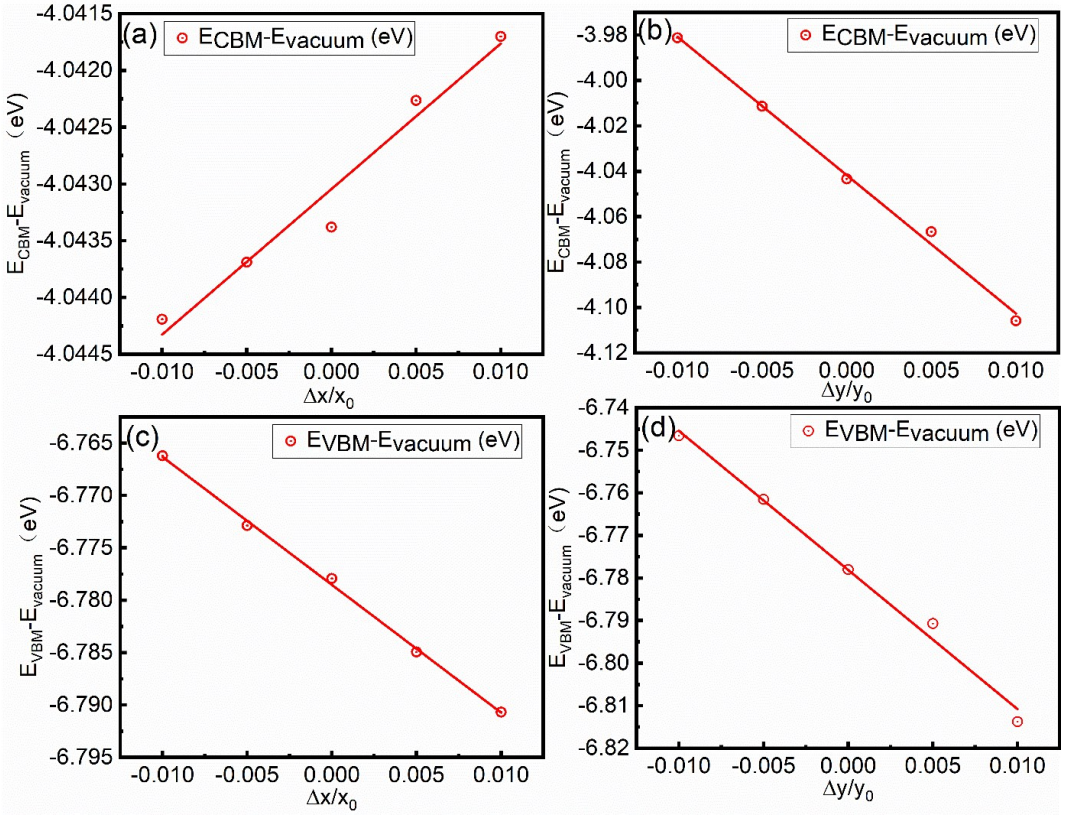

Fig. S7 Typical fitting results in the evaluation of E_d (of electron state and hole state) of monolayer InTeI along *x*-direction (a, c) and *y*-direction (b, d), respectively. The slope is the deformation potential E_d.

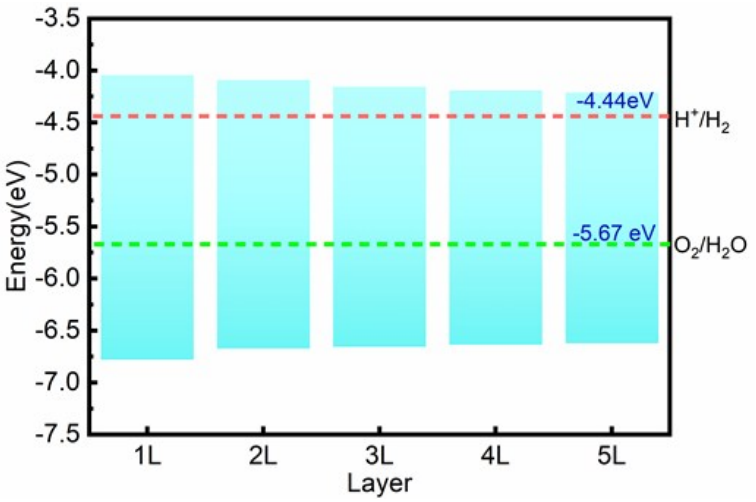

Fig. S8 Locations of VBM and CBM in the band structures of InTeI monolayer and multilayers based on HSE06 functionals, in relative to the energy level of vacuum. The chemical reaction potentials for H^+/H_2 and O_2/H_2O (at pH = 0) are indicated with the dashed lines.

Table S2 Energy conversion efficiency of light absorption (η_{abs}), carrier utilization (η_{cu}), and solar-to-hydrogen (η_{STH}) of monolayer and multilayer InTeI systems.

N_L	η_{abs} (%)	η_{cu} (%)	η_{STH} (%)
1L	10.79	39.72	4.29
2L	15.46	41.70	6.44
3L	17.62	42.52	7.49
4L	18.87	42.98	8.11
5L	20.10	43.43	8.73

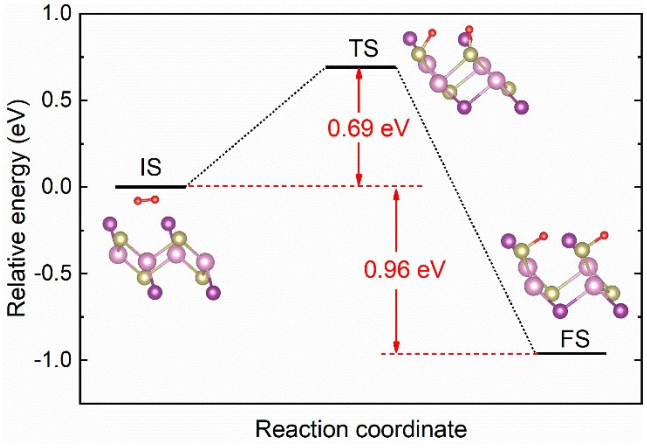

Fig. S9 Reaction pathway for a physisorbed O_2 to dissociate and form O−Te bond over monolayer InTeI. IS, TS, and FS stand for the initial state, transition state, and final state of the oxidation processes, respectively. The insets are the configurations of different states.